The Meteoritical Society

Meteoritics & Planetary Science 1–18 (2021)
doi: 10.1111/maps.13651

How do secondary iron enrichments form within basaltic eucrites? An experimental approach

Stella ROMBECK[1], Christian VOLLMER[1]*, Julia ROSZJAR[2], Adam R. SARAFIAN[3], and Stephan KLEMME[1]

[1]Institut für Mineralogie, Westfälische Wilhelms-Universität Münster, Corrensstrasse 24, 48149 Münster, Germany
[2]Department of Mineralogy and Petrography, Natural History Museum Vienna, Burgring 7, 1010 Vienna, Austria
[3]Corning Incorporated, Science and Technology Division, 21 Lynn Morse Rd., Painted Post, New York 14870, USA
*Corresponding author. E-mail: christian.vollmer@wwu.de

(Received 10 June 2020; revision accepted 16 March 2021)

Abstract–Some basaltic eucrites and basaltic lithologies in howardites derived from the asteroid 4 Vesta exhibit unusual secondary veinlet textures consisting mostly of fayalitic olivine and Fe-enrichments within pyroxenes. Recent studies discussed the formation of these Fe-rich phases either by interaction with a vapor and/or liquid phase (metasomatism), or by a high-temperature melting process. We therefore performed a series of heating and hydrothermal experiments with liquids of different compositions on natural pyroxene crystals (augite and orthopyroxene) to evaluate these contrasting hypotheses. The results of the heating experiments show that incongruent melting of pyroxenes at about 1070 °C causes textures that are very similar to those observed in the meteorites. We conclude that a part of the natural secondary veins might be explained by heating processes at similar temperatures. The hydrothermal experiments with aqueous liquids of different Fe-enriched compositions clearly indicate ion exchange reactions resulting in partial Fe-enrichments of the pyroxene. Interestingly, these Fe-enrichments occurred independent of the Fe content of the liquid, which can be explained by an internal origin of Fe from the pyroxenes. In one hydrothermal experiment of augite with Fe-oxalate solution, deposition of fayalitic olivine was observed. From our experimental observations, we conclude that aqueous liquids are plausible candidates for explaining the deposition of Fe-enrichments and fayalitic olivine inside the fractures of pyroxene. However, we cannot rule out a high-temperature melting process slightly above the peritectic point of pyroxene to explain a fraction of observed secondary Fe-enrichments.

INTRODUCTION

Eucrites belong to the suite of HED meteorites (howardites, eucrites, and diogenites) representing the largest suite of achondrites (Pun and Papike 1996; Mittlefehldt 2015), which currently encompass 2287 classified meteorites according to the Meteoritical Bulletin (June 9, 2020). HED meteorites most likely formed about 4.56 Ga ago on the differentiated asteroid 4 Vesta ("Vesta" hereafter) during a complex combination of mostly magmatic activity and impact processes. The crustal rocks were mechanically stressed, brecciated, mixed together due to impact processes, and exposed to various degrees of thermal annealing and metamorphism. These processes resulted in a continuous change in petrographic characteristics and led to the formation of highly complex and heterogeneous breccias, with fragments of different lithologies (polymict breccias), showing postmagmatic features of different intensities (Consolmagno and Drake 1977; Drake 1979, 2001; Binzel and Xu 1993; Metzler et al. 1995; Pun and Papike 1996; Yamaguchi et al. 1996; Binzel et al. 1997; Gaffey 1997; Papike 1998; McCoy et al. 2014; Vollmer et al. 2020).

In addition to these well-known processes, a limited number of samples, with basaltic eucrites and some

eucrite clasts in howardites in particular, contain some unusual veinlet-like mineral parageneses that cannot be easily explained by the processes summarized above (e.g., Treiman et al. 2004; Schwartz and McCallum 2005; Barrat et al. 2011; Roszjar et al. 2011; Sarafian et al. 2013, 2017; Warren et al. 2014, 2017; Pang et al. 2017; Patzer and McSween 2018; Roszjar 2019; Vollmer et al. 2020). These secondary textures include (1) quartz veinlets, e.g., within the Serra de Magé cumulate eucrite (Treiman et al. 2004); (2) apatite veinlets and or apatite-merrillite replacement reactions in, e.g., Juvinas, Northwest Africa (NWA) 5073, or the Serra Pelada basaltic eucrite (e.g., Roszjar et al. 2011; Sarafian et al. 2013; Roszjar 2019); (3) secondary Fe metal, in, e.g., Camel Donga and NWA 5738 (Warren et al. 2014, 2017); and (4) Fe-enrichments and/or veinlet-like textures mainly composed of fayalitic olivine in, e.g., Pasamonte, NWA 049/1000/1109/2061/5073/5738, Yamato (Y)-75011/82202 basaltic eucrites (Takeda et al. 1983, 1994; Warren 2002; Barrat et al. 2011; Roszjar et al. 2011; Warren et al. 2014; Pang et al. 2017; Vollmer et al. 2020) and in Allan Hills (ALH) 09004, LaPaz Icefield (LAP) 04838, and Miller Range (MIL) 07007 howardites (Patzer and McSween 2018). These Fe-enrichments mostly occur along cracks crosscutting both unequilibrated and equilibrated pyroxenes and are in some cases accompanied by small amounts of anorthitic plagioclase and small troilite or chromite grains. Evidently, these phases postdate the main magmatic history of the rock and formed on the parent body (Takeda et al. 1983, 1994; Warren 2002; Roszjar et al. 2009, 2011; Barrat et al. 2011; Barrett et al. 2016; Pang et al. 2017; Patzer and McSween 2018; Vollmer et al. 2020). Petrographic and mineralogical characteristics indicate that the formation of these secondary phases requires processes under various low- and high-temperature conditions. The general makeup of the secondary alteration features seems to be independent of the degree of metamorphism and therefore may have happened during several stages of postmagmatic evolution (e.g., Pang et al. 2017; Vollmer et al. 2020). Strikingly similar alteration effects and olivine veinlets have also been reported recently in lunar rocks (Warren et al. 2018; Zeng et al. 2020).

The physicochemical processes leading to these veinlet-like textures are controversially debated. Current discussions comprise several theories based on two fundamentally different processes including (1) metasomatic reaction of a liquid or gas phase with minerals (Takeda et al. 1983; Mittlefehldt and Lindstrom 1997; Warren 2002; Barrat et al. 2011); (2) a high-temperature process, such as incongruent melting of the pyroxenes and formation of a highly fractionated Fe-rich magma (e.g., Roszjar et al. 2011; Patzer and McSween 2018). Initially, Vesta was assumed to be an asteroid devoid of large amounts of volatiles and hence without aqueous liquids, which seemed to rule out a liquid phase as the major metasomatic agent involved in the formation process (Mittlefehldt 2015). No evidence for the existence of hydrous minerals such as sheet silicates or clays has been found within HED meteorites. However, recent remote sensing data revealed the presence of hydrogen or phyllosilicates on the asteroid's surface, which is good evidence for the fact that aqueous liquids may indeed be present within Vesta's crust (Hasegawa et al. 2003; Denevi et al. 2012; Prettyman et al. 2012). Therefore, secondary alteration by interaction with such hydrothermal liquids has been proposed as an important process on the surface of Vesta (e.g., Sarafian et al. 2013, 2017).

In this study, we performed a series of heating and hydrothermal experiments on natural rock-forming pyroxene minerals to test whether hydrothermal or magmatic processes are more likely responsible for the formation of secondary ferroan pyroxenes in HED meteorites. Our experimental strategy was to test the aforementioned hypotheses, and we will use our experimental results to interpret the surface processes that occurred on the HED parent body.

EXPERIMENTAL METHODS

Starting Materials

We performed experiments with pyroxene starting material only, provided by the Natural History Museum, Vienna, Austria. Secondary Fe-rich phases in eucrites occur in pyroxene only, and previous studies suggested that no additional minerals were involved in the formation process (e.g., Barrat et al. 2011). We used terrestrial pyroxene of different compositions: orthopyroxene (En_{68}, abbreviated with "Hy" in the table because of its "hypersthene" composition and named "orthopyroxene" hereafter, originating from Mäntyharju, Finland), and augite ("A"), originating from an olivine-pyroxene basalt from Pico, the highest volcano of the Azores, Portugal. Augite is homogeneous with a mean chemical composition of $(Ca_{0.88}Na_{0.03}Fe_{0.13})_{1.04}(Mg_{0.88}Al_{0.05}Ti_{0.12})_{1.05}(Si_{1.92}Al_{0.08})_2O_6$. Several small inclusions of olivine (Fo_{76}), ilmenite, spinel, and antiperthitic feldspar (Ab_{93}) with orthoclase exsolutions are present. The orthopyroxene crystals are also homogeneous with a chemical composition of $(Mg_{1.2}Fe_{0.56}Ca_{0.02}Mn_{0.01}Ti_{0.01}Al_{0.14})(Si_{1.88}Al_{0.12}O_6)$ and evenly distributed exsolution lamellae of about 15 μm width. These minerals were cut into 1 mm^3 sized cubes, using a slow-speed diamond wheel saw.

Heating Experiments

Heating experimental series were performed following the considerations of Roszjar et al. (2011), who proposed that incongruent in situ melting of primary pigeonitic pyroxene in the NWA 5073 eucrite may have formed Fe-enrichments. They suggested that temperatures slightly above the peritectic were needed to achieve formation of these features. We chose the experimental temperatures following classical phase diagram information (Bowen and Anderson 1914; Grieg 1927; Bowen and Schairer 1934). All experiments were performed at the Institut für Mineralogie, Universität Münster, in gas-mixing furnaces at atmospheric pressure (1 atm) to be as close as possible to Vesta-like surface pressures. We flushed the furnace with inert argon gas to avoid an oxidation or reduction reaction of the starting materials with the atmosphere, which we believe is similar to the case of Vesta with a lack of atmosphere. However, note that the experiments were unbuffered with regard to oxygen fugacity. The pyroxene cubes were placed on a platinum holder and suspended into the hot furnace. Experimental run durations and temperatures ranged from 70–330 min and 1070–1350 °C. The experiments were rapidly quenched in air by fast extraction out of the furnace. In order to assess a possible influence of the quenching method, a few experiments were repeated with a different extraction speed from the furnace, different run durations, and one run was conducted with a slower cooling rate. Details of the experimental run conditions and starting materials are given in Table 1.

Table 1. Conditions of high-temperature experiments.

Experiment	Temperature (°C)	Gas flow (ccm/min)	Duration (min)	Cooling rate
Augite				
E1_S_A	1070	115	195	Quenched
E2_S_A	1170	140	195	Quenched
E9_S_A	1300	200	70	Quenched
E10_S_A	1250	200	70	Quenched
E13_S_A	1350	200	70	Quenched
Orthopyroxene ("Hypersthene")				
E1_S_Hy	1070	115	195	Quenched
E2_S_Hy	1170	140	195	Quenched
E11_S_Hy	1070	200	195	1.5°C min^{-1}
E3_S_Hy	1070	115	330	Quenched
E4_S_Hy	1300	115	70	Quenched
E5_S_Hy	1280	115	70	Quenched
E6_S_Hy	1320	115	70	Quenched
E7_S_Hy	1300	115	20	Quenched
E8_S_Hy	1300	115	150	Quenched
E9_S_Hy	1300	200	70	Quenched

Hydrothermal Experiments

Hydrothermal experiments were designed following suggestions that an Fe-rich liquid could be responsible for the formation of Fe-rich phases in pyroxene (e.g., Herd et al. 2004; Barrat et al. 2011). Since the nature, origin, and chemical composition of this liquid on the HED parent body are unknown, experiments were run with liquids of different chemical compositions. Some runs were conducted with distilled water to evaluate whether the Fe source was within the pyroxenes themselves, and other runs were performed with Fe-rich liquids, analogous to an open system model suggested by Barrat et al. (2011). The Fe-rich liquids are, naturally, the source of Fe so that secondary phases originate from an endogenous source (e.g., magmatic gases) or exogenic liquid phase (e.g., volatile- and Fe-rich impactor material). Our Fe-rich aqueous liquids contain Fe-oxalate ($FeC_2O_4*2H_2O$) and Fe-chloride ($FeCl_2$), both prepared with 4 g material per 70 ml distilled water. Furthermore, we mixed distilled water with hydrochloric acid (HCl) to pH values of about 2 to enhance the reaction rate. We also used a solution of Fe-fluoride (FeF_2*3H_2O), which notably changed its color rapidly after mixing from clear to red, which may be the result of instant oxidation before the start of the run.

Hydrothermal experiments were performed at temperatures of 200 °C. Each pyroxene cube was inserted into a cylindrical Teflon®-lined reactor (12 mm diameter, 28 mm height) with a lid, together with 1 mL of liquid. The Teflon® reactor was gently pressed into a steel autoclave and tightly sealed to avoid any liquid loss during the run. The pressure was generated autogenously when the steel autoclave was placed in a custom-made low-temperature furnace. After the run, the autoclaves were removed from the furnace and quickly cooled in a flow of compressed air to room temperature (~22 °C). The sample's weight and the liquid's pH value were measured before and after the experiment to document possible material loss or gain (see Table 2).

As Vesta's surface temperature is <0 °C, reaction rates are assumed to be very slow (DeSanctis et al. 2012). As experimental reaction rates in the laboratory need to be much faster, we chose to run experiments at 200 °C to enhance reaction rates. We stress that the type of reaction is not likely to be affected by the increase in temperature. In addition to separate heating and hydrothermal experiments, we also combined both experimental methods and performed a heating

Table 2. Conditions of hydrothermal experiments.

Experiment		Sample		Fluid					
Sample	Duration (weeks)	$Weight_i$ (g)	$Weight_f$ (g)	Composition	Formula	pH_i	pH_f	$Appearance_i$	$Appearance_f$
E1.1_H_A2	2	0.0084	0.0053	Iron chloride	$FeCl_2$	1.4	<1	Rusty-red	Light yellow, dark residue in the Teflon container
E1.2_H_A1	7	0.0052	0.0019	Iron chloride	$FeCl_2$	1.4	<1	Rusty-red	Light yellow, dark residue in the Teflon container
E1.1_H_A4	2	0.0063	0.0061	Iron oxalate	$FeC_2O_4 * 2H_2O$	5.3	8.4	Light yellow	Clear, with red particles
E1.2_H_A3	7	0.0029	0.0029	Iron oxalate	$FeC_2O_4 * 2H_2O$	5.3	6.9	Light yellow	Clear, with red particles
E2_H_A7	5	0.0036	0.0022	Iron fluoride	FeF_2*3H_2O	3.5	2–2.5	Milky	Slightly reddish, rust brown residue
E2_H_A9	5	0.0032	0.0022	Hydrochloric acid	$H_2O + HCl$	~2	~6	Clear	Reddish
E3_H_Hy	4	0.0019	–	Hydrochloric acid	$H_2O + HCl$	~2	2	Clear	Clear with green splinters, sample decayed
E1.1_H_A6	2	0.0033	0.0032	Dist. water	H_2O	~7	8.6	Clear	Clear
E1.2_H_A5	7	0.0051	0.0050	Dist. water	H_2O	~7	7.9	Clear	Clear
E2_H_Hy	6	0.0034	0.0033	Dist. water	H_2O	~7	~7	Clear	Clear with green splinters
E4_H_Hy	4	0.0039	0.0038	Dist. water	H_2O	~7	~7	Clear	Clear

i = initial, f = final, Dist. = Distilled water.

experiment followed by a hydrothermal treatment (Tables 1 and 2).

Sample Preparation and Analytical Techniques

After completion of the experiments, samples were embedded in epoxy resin mounts, polished, and carbon coated for electron beam analysis. Samples were investigated with a JEOL 6510-LA scanning electron microscope (SEM) equipped with a W-electron emitter and a backscattered electron (BSE) detector at the Institut für Mineralogie, Münster. All analyses were performed with an accelerating voltage of 20 kV, a working distance of 10 mm, and a beam current of several nA. We also identified and analyzed respective reaction products semiquantitatively by a silicon-drift energy-dispersive X-ray detector attached to the SEM using theoretical k factors.

RESULTS

Heating Experiments

Augite Starting Material

BSE images of high-temperature experimental products with augite starting material confirm that incongruent melting begins at around 1250 °C with a run duration of 70 min (E10_S_A, Fig. 1). In our runs, we observed that melt pockets with diameters of about 100 μm and homogeneous composition start to form at grain margins. These initial melts are enriched in Na, Al, Fe, and Ti, and depleted in Mg, Si, and Ca compared to the augite composition. Small (~4 μm) Fe-Cr-rich spinels also formed within the melt. Experimental results at lower temperatures showed no indication for melt generation (E1_S_A, E2_S_A). However, primary augite inclusions disappeared at an experimental temperature of about 1170 °C (E2_S_A). With increasing temperature (up to 1350 °C), melt pockets increased in size, and became more augite-like in composition and texturally more complex (Figs. 1b and 1c).

Orthopyroxene Starting Material

The response of orthopyroxene to heating was observed at around 1070 °C (Fig. 2). BSE images of the run products of experiment E1_S_Hy document the formation of small cracks within the margin of the crystal, forming a network of SiO_2-rich and Fe, Ti-rich veins with aligned sub-μm-sized crystals, probably spinel phases (Figs. 2a and 2b). The reaction rim was about 50 μm wide, and sizes of exsolution lamellae widened in

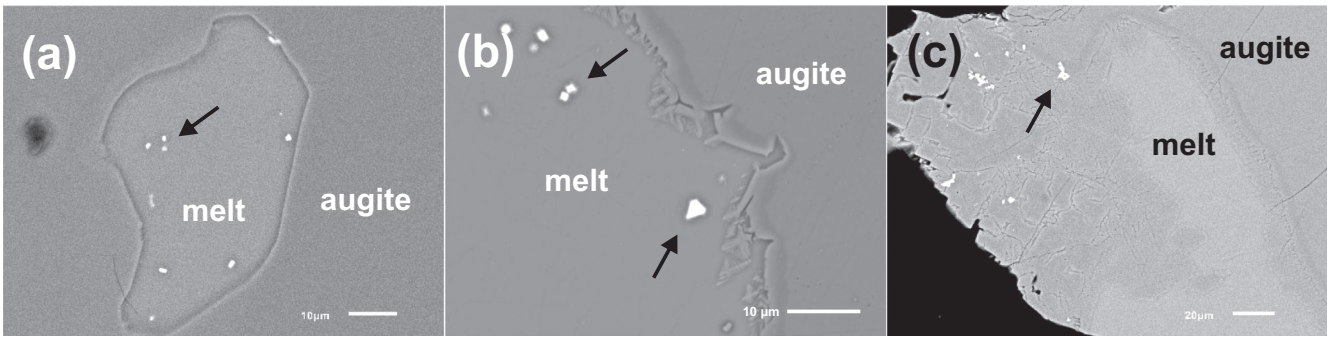

Fig. 1. BSE images of augite material heated at (a) 1250 °C for 70 min (E10_S_A), (b) 1300 °C for 70 min (E9_S_A), and (c) 1350 °C for 70 min (E13_S_A). The results show a successful melting process and the formation of most likely spinel-type phases (arrow-marked).

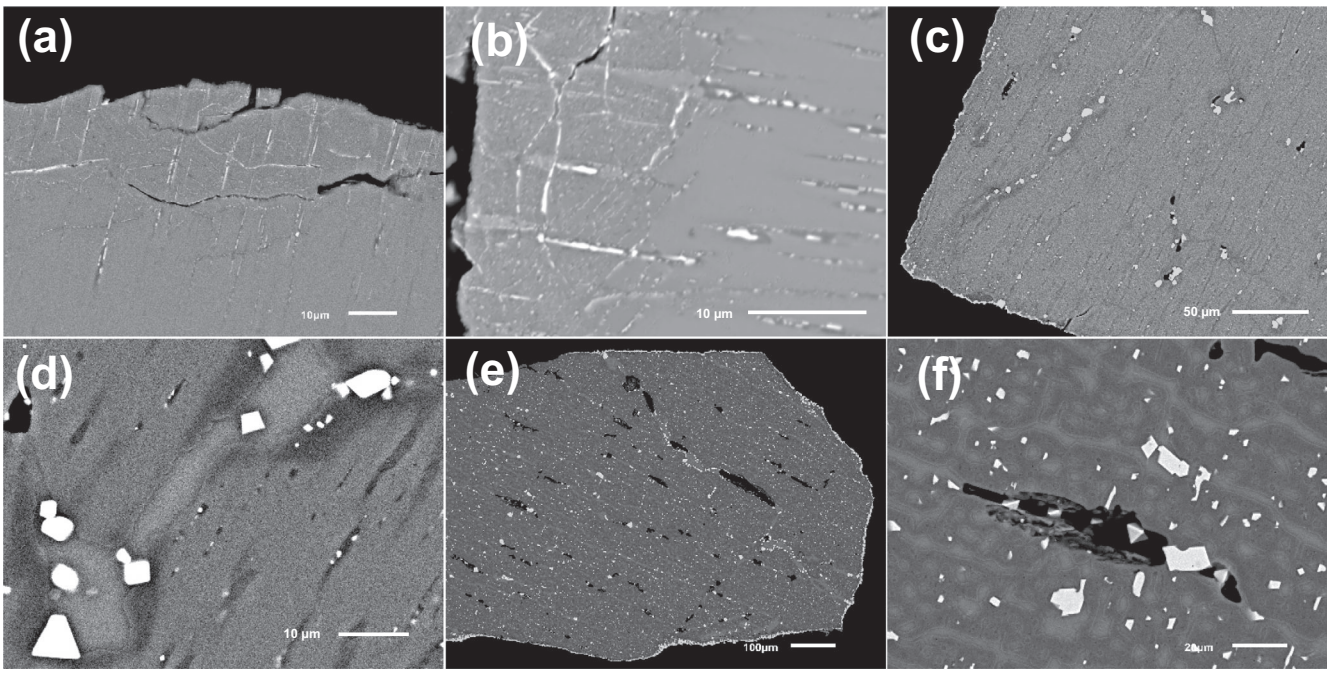

Fig. 2. BSE images of heating experiments with orthopyroxene material (a, b) heated at 1070 °C for 195 min (E1_S_Hy). Small cracks form a network of SiO_2-rich and Fe, Ti-rich veins and aligned crystals. c, d) At 1170 °C for 195 min (E2_S_Hy), Mg, Si-rich areas form together with a Ca, Ti, Al-rich melt a network including small Fe, Ti-rich spinels and isolated cavities. e, f) At 1300 °C for 70 min (E4_S_Hy), extensive melt production, cavities, and Fe, Ti-rich spinels formed.

this rim. The experiments at the same temperature, but longer duration (E3_S_Hy) or a slower cooling rate (1.5 °C min^{-1}) revealed similar results. Alignment of the Fe- and Ti-rich veins suggests a crystallographic relationship with the host pyroxene. The small Fe-Ti-rich crystals are generally surrounded by an SiO_2-rich phase or accumulated along the edges of cavities. In the center of the samples, the orthopyroxene crystals kept their initial composition with typical exsolution lamellae. Compared to the initial orthopyroxene composition, the region surrounding Fe-Ti-rich phases was slightly enriched in MgO and depleted in FeO, clearly indicated in BSE images (Figs. 2c and 2d).

At 1170 °C (E2_S_Hy), the reaction of orthopyroxene was much more pronounced and occurred throughout the entire sample (Figs. 2c and 2d). In BSE images, dark gray Mg- and Si-rich areas together with brighter Ca, Ti, and Al-rich areas formed a melt network across the whole grain. In these areas, small Fe- and Ti-rich spinels with diameters of up to 15 µm formed, mostly in a defined crystallographic orientation to the host pyroxene and along cleavage

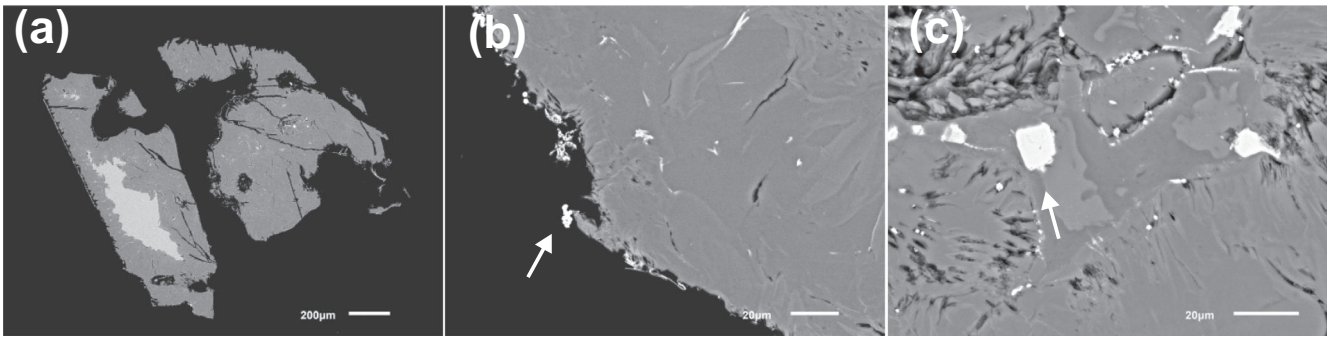

Fig. 3. BSE images of hydrothermal experiments of augite material reacted with an Fe-chloride solution (E1.1_H_A2, E1.2_H_A1). a) Reaction rim consisting of almost pure SiO_2. Rutile-like phases (b) and Fe-rich phases presumably magnetite (c) are located within the reaction product (arrow-marked).

planes. Furthermore, isolated cavities and enhanced porosity was formed, which likely led to enhanced reaction rates. During experimental series E4_S_Hy–E9_S_Hy, temperature and duration varied between 1280–1320 °C and 20–150 min. In all of these experiments, extensive melt production as well as development of cavities and crystallization of Fe, Ti-rich spinel-like phases occurred. Compared to the initial pyroxene, the melt was significantly enriched in Al and Ca, but depleted in Mg and Fe, while the corresponding pyroxene was significantly enriched in Mg and Si, clearly visible in BSE images (Figs. 2e and 2f).

Hydrothermal Experiments

In general, samples of hydrothermal experiments showed clear reaction rims, indicating a successful interaction between liquid and mineral. Some runs lost small amounts of liquid during the run, but we assume that the loss was not significant and did not affect the experimental results.

Augite + Fe-chloride

The reaction of augite with Fe-chloride solution (E1.1_H_A2, E1.2_H_A1; Fig. 3) generated clear reaction rims, which grew in size with increasing run duration. The reaction also changed the color of the liquid from rusty brown to light yellow and formed a black, sparkling residue in the Teflon® container. Based on SEM-EDS analysis, this residue consisted of mainly Cl and Fe. The reaction product was fibrous, showed cavities, and consisted almost entirely of SiO_2, with some areas containing about 2 wt% Al_2O_3. The original feldspar inclusions within the starting augite did not react with the solution. However, we observed newly formed acicular rutile crystals as well as spherical Fe-rich phases with diameters of a few µm, presumably magnetite (Figs. 3b and 3c). Note that all the aforementioned phases were too small to be properly analyzed by SEM-EDX.

Augite + Fe-oxalate

A longer experimental run duration with Fe-oxalate solution (E1.1_H_A4, E1.2_H_A3) did not show a significant increase in the reaction rate (Figs. 4a and 4b). However, the pH of the liquid was slightly more basic after the experiments and the liquid changed color from light yellow to slightly reddish and contained small particles. However, particularly striking here was that a feldspar inclusion located on the edge of the sample strongly reacted with the liquid (Figs. 4a and 4b). At the boundary between pyroxene and feldspar, Fe-rich olivine grains of ≤5 µm diameter were observed together with Fe-Ti-rich spinels.

Augite + Fe-fluoride

After the reaction with Fe-fluoride (E2_H_A7, 5 weeks), the entire augite crystal had reacted and showed numerous cavities. The liquid changed its color from milky white to slightly reddish after the experiment. BSE images showed complex intergrowths of Mg-fluoride (MgF_2), Ca-fluoride (CaF_2), and spinel-like phases (Fig. 4c).

Augite + Hydrochloric Acid

The reaction of augite with HCl led to a slight loss of material (E2_H_A9, Figs. 4d and 4e). The color of the liquid changed from transparent to slightly reddish and its pH changed from 2 to about 6. Elongated areas of ilmenite-like composition formed at the sample's margin, frequently surrounded by very fine Al-rich acicular crystals. In addition, cloudy phases rich in Si and Al formed (Figs. 4d and 4e).

Augite + Distilled Water

After the reaction of augite with distilled water (E1.1_H_A6, E1.2_H_A5), Al-rich and spinel-like products apparently formed within the brittle edges of the sample cube. In the marginal area, inclusions were observed, which evidently interacted with the liquid more rapidly than the

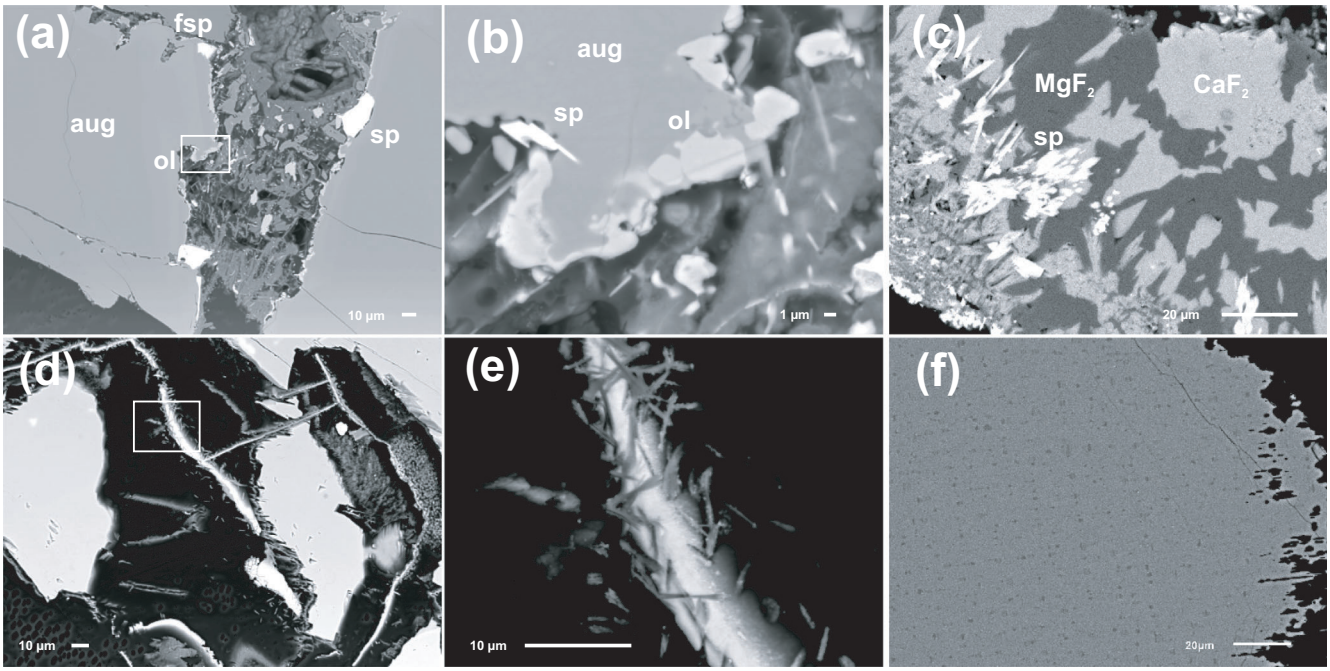

Fig. 4. BSE images of hydrothermal experiments. a, b) Augite material reacted with an Fe-oxalate solution (E1.1_H_A4, E1.2_H_A3). A strongly reacted inclusion contains Fe-rich olivines, Fe, Ti-rich phases, and spinel-like products. c) Augite material reacted with an Fe-fluoride solution (E2_H_A7) showing the reaction products spinel, Mg-fluoride, and Ca-fluoride. d) Augite material reacted with hydrochloric acid (HCl; E2_H_A9) showing elongated areas of ilmenite-like composition (marked by the box). e) Magnified view of the box in (d), in which very fine Al-rich needles surround ilmenite-like areas. f) Orthopyroxene material reacted with HCl (E3_H_Hy) showing a distinct reaction margin.

pyroxene and have an Fe-rich composition (Figs. 5a and 5b).

Orthopyroxene + Hydrochloric Acid

During the reaction of orthopyroxene with HCl (E3_H_Hy), the solution did not change noticeably in color. However, BSE images showed a distinct reaction rim with slightly increased values of Fe, Mg, and Cl (Fig. 4f).

Orthopyroxene + Distilled Water

This run (E2_H_Hy) experienced little weight loss, and the liquid's pH remained the same. In BSE images, fine acicular phases were observed within fracture voids possibly generated by the mechanical stress due to previous preparation steps. These phases were aligned and showed significant Fe accumulation (Figs. 5c and 5d).

Combined Experiment

The combined run with orthopyroxene (E4_H_Hy) showed a slight material loss, but the liquid's color did not change. BSE images reveal a reaction zone at the rim of the crystal extending into the center of the pyroxene and forming fibrous and/or Fe-rich and spinel-like phases. The orthopyroxene close to the reaction rim looked unaffected, but had high concentrations of Fe. In addition, exsolution lamellae close to the sample edge coarsened, void spaces were abundant, and small Fe-rich phases precipitated (Figs. 5e and 5f).

DISCUSSION

Heating Experiments with Augite and Orthopyroxene

The results of the heating experimental series with augite showed no textural features similar to those observed in naturally occurring secondary phases in basaltic eucrites. Therefore, it appears that at least short-term heating above the solidus of augite cannot explain the formation of Fe-enrichments in basaltic eucrites. Heating experiments with orthopyroxene starting material at temperatures of 1070 °C (E1_S_Hy, E3_S_Hy), however, showed reactions restricted to the edges of the sample cube. Notably, this marginal reaction may be assigned to mechanical fractures that formed during sample cube preparation along the mineral cleavage. Nevertheless, the textures observed in the orthopyroxene melting experiments strongly resemble the textures of some of the secondary features found within eucrites, specifically Fe-enrichments within basaltic

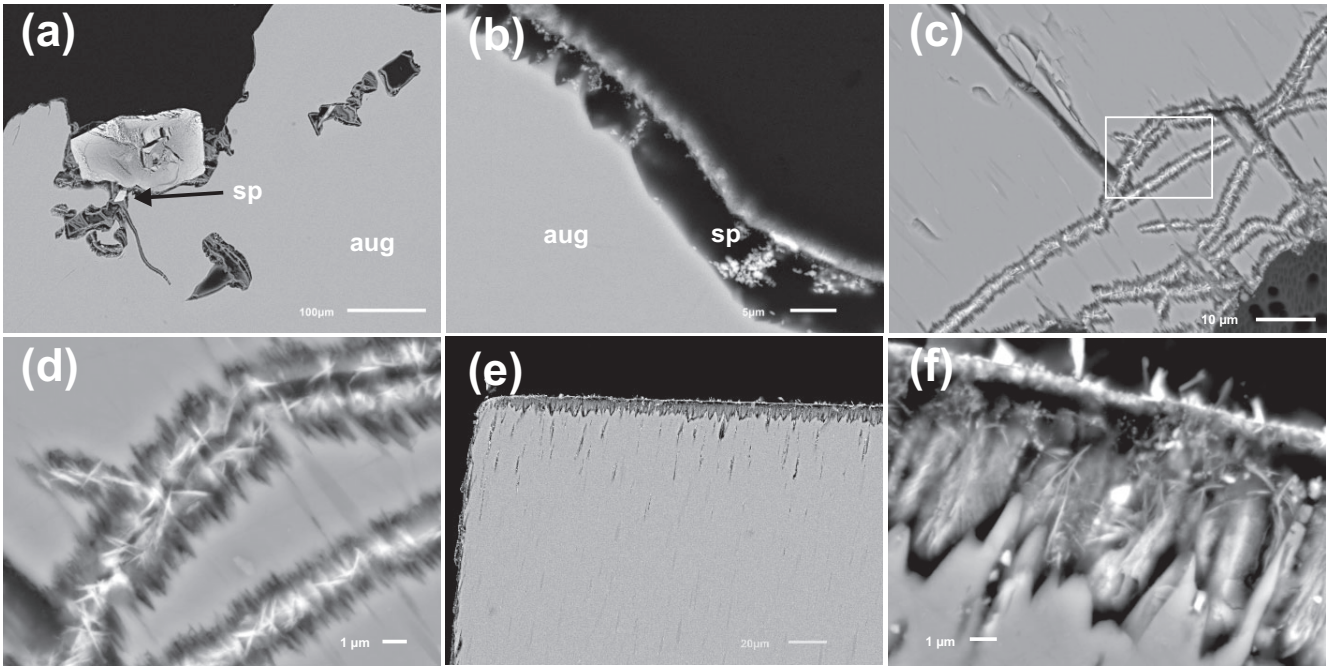

Fig. 5. BSE images of hydrothermal experiments. a, b) Augite material reacted with distilled water (E1.1_H_A6, E1.2_H_A5) showing a strongly reacted Fe-rich inclusion and Al-rich and/or spinel-like reaction products. c, d) Orthopyroxene material reacted with distilled water (E2_H_Hy) showing fine, Fe-rich acicular phases located in the voids of fractures. e, f) Orthopyroxene material heated at 1070 °C for 195 min (E4_H_Hy) and afterward reacted with distilled water (E_S_11) showing a strong reaction margin with Fe-rich phases.

pyroxenes (Fig. 6). We therefore argue that naturally occurring secondary Fe-enrichments within eucritic pyroxenes may be due to such short-term heating events slightly above the peritectic temperature of around 1070 °C. The heat source could be due to widespread shock events and basaltic magmatic activity on Vesta, possibly generated by Al-26 decay (Yamaguchi et al. 1996; Roszjar et al. 2011). A longer duration of the experiment did not result in a textural change, but more pronounced element enrichments or depletions. A cooling rate of 1.5 °C min^{-1} also had no significant effect (E11_S_Hy, Fig. 2).

The experiments at 1070 °C showed that during melting Fe and Ti were released from the pyroxene first, which resulted in magnetite- or spinel-like droplets or veins in cavities or along crystal lattice surfaces and a more residual Mg-rich pyroxene (Figs. 1 and 2). Yamaguchi and Mikouchi (2005) and Yamaguchi et al. (2013) described a similar observation in a series of experiments on basaltic eucrites, where a Ti-rich melt (~1% melt fraction) formed along grain boundaries and within cracks at temperatures of around 1070 °C. At 1170 °C, the entire orthopyroxene cube reacted and larger melt pools, spinel-type phases, and cavities formed (E2_S_Hy, Fig. 2). During the melting process, Fe, Ti, Al, and Ca are incompatible and hence, a more Mg-rich residual pyroxene developed. Iron and other elements like Ti formed a spinel-like phase, most likely magnetite (Fe_3O_4). This is also very similar to observations in eucrites (Fig. 6). Note that our experiments were run in an inert atmosphere intended to simulate conditions on Vesta, i.e., a planetary body without atmosphere. However, as our experimental starting material contained some Fe^{3+}, magnetite formation in our experiments can be explained by intrinsic oxygen fugacities of the starting materials. Experiments at ~1300 °C resulted in ~50% melting, and a different run duration only had a minor effect on the chemical and physical properties of the initial orthopyroxene material (Table 1). Temperature changes had no impact on this result.

In summary, our experimental heating series on orthopyroxene starting material could partly reproduce naturally occurring secondary alteration features, with Fe-enrichments observed in basaltic pyroxenes in particular (Fig. 6). We found texturally comparable results with regard to the Fe-enrichments in eucrites when orthopyroxene was slightly heated above its peritectic point of about 1070 °C (Fig. 6).

Hydrothermal Experiments

The mechanism of transformation from one solid phase to another is driven by disequilibrium of the

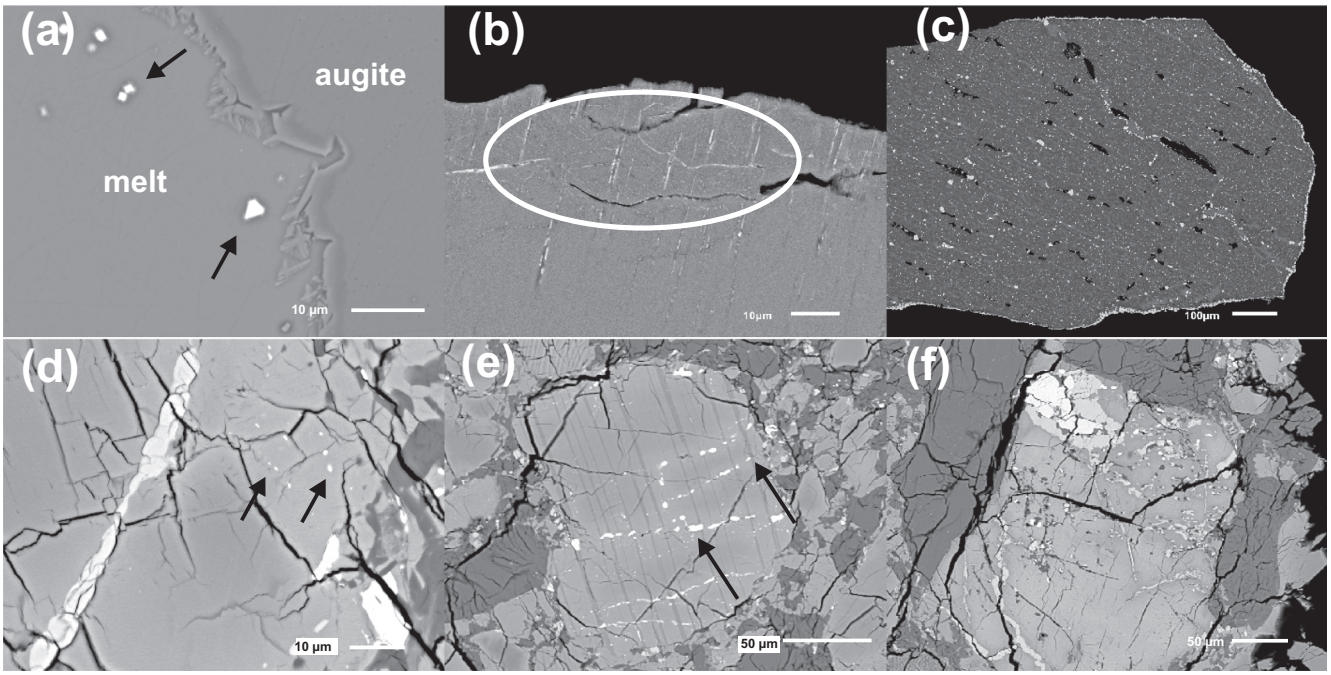

Fig. 6. BSE images of heating experimental results from this study (a–c) in comparison with natural pyroxenes in selected Yamato eucrites described in Vollmer et al. (2020). Textures of natural secondary alteration phases are partly similar to experimental results (d–f). a) Augite heating experiment E9_S_A (1300 °C for 70 min) with exsolved small spinel-like phases (arrow-marked). b) High-temperature orthopyroxene experiment E1_S_Hy (1070 °C), showing Fe, Ti-rich structures (encircled) in a regular pattern in the rim of the crystal. c) High-temperature orthopyroxene experiment E4_S_Hy, heated at 1300 °C for 70 min, with extensive melt production, cavities, and Fe- and Ti-rich spinels throughout the entire crystal. d) Prominent fayalite vein crosscutting a fractured pyroxene grain within eucrite Y-75011. However, some smaller Fe-Ti-rich inclusions can be observed as well (arrow-marked), similar to observations in experiments (a). e) Aligned Fe-Ti-rich phases (arrow-marked) within pyroxene in polymict eucrite Y-74450 in a similar pattern as in experiments (b). Note that aligned phases crosscut exsolution lamellae and are less regular compared to experiments. f) Patchy Fe-rich inclusions (fayalite, Fe-Ti-rich phases, and anorthite) within pyroxene in the polymict eucrite Y-74159 in a roughly similar, chaotic texture as in (c). However, melt development such as in the experimental run is not observed.

system caused by changes in physical and chemical conditions such as liquid composition. In order to re-establish the state of equilibrium, reactions resulting in chemical and/or textural changes have to take place (Putnis and Putnis 2007). According to Cardew and Davey (1985), a metastable phase can dissolve in such a reaction and a more stable phase can grow or precipitate simultaneously. The exchange reaction starts with the dissolution of the uppermost molecular layers of the metastable phase and produces a significant supersaturation of the liquid in direct contact with the crystal, resulting in the precipitation of a new, more stable phase and ion exchange reactions with both structural and chemical changes. The process is therefore based on a coupled dissolution–precipitation reaction (Putnis and Putnis 2007). If the reaction product has a lower molecular volume and lower solubility, the exchange results in enhanced porosity, which acts as a pathway for the liquid to the inner metastable phase and, hence, proceeding reaction. In almost all hydrothermal experiments of this study, a slight loss of material and a change in pH of the liquid could be detected, which indicates a clear ion exchange reaction. This is a very important finding concerning our hydrothermal experiments and demonstrates the significance of those exchange reactions.

The reaction of augite with Fe-chloride (E1.1_H_A2 and E1.2_H_A1) led to the formation of a well-defined reaction rim. The porous rim consisted almost exclusively of Si with minor Al, which is most likely due to a leaching process. During leaching, components are dissolved from the solid phase by the liquid and precipitate elsewhere (Putnis and Putnis 2007). In addition, leaching may involve the incorporation of other components from the liquid, e.g., oxygen, which in this case cannot be evaluated. The newly formed Ti-rich phases indicate the precipitation of a new phase from the liquid. The absence of Fe and Cl indicates that these ions only served as actors during the reaction.

The reaction with Fe-fluoride (E2_H_A7) resulted in a complete transformation of the initially homogeneous pyroxene into a porous material

consisting of Mg-fluoride, Ca-fluoride, and spinel. Pyroxene completely dissolved and new phases formed by reaction with the liquid. The formation of two different phases (MgF_2 and CaF_2) suggests that the structural similarities between old and new phases were very small, in agreement with previous studies (e.g., Putnis and Putnis 2007).

The reaction of augite with Fe-oxalate clearly showed that the feldspar inclusion reacted with the liquid much more extensively than the pyroxene. The dissolution of the feldspar may have caused a strong chemical disequilibrium between pyroxene and liquid. This resulted in the dissolution of pyroxene and the formation of serpentine-like phases and Fe-rich olivine. The olivines in this run showed texturally similar properties to secondary olivine in eucrites (Fig. 7); they were located along pyroxene margins, had a granular shape, and were very Fe-rich ($Fa_{>69}$).

HCl was used to promote the reaction between pyroxene and liquid (E3_H_Hy, E2_H_A9, Fig. 4), and the observed extensive reaction supports the observation that pH values changed significantly during experiments. Both runs contained pyroxenes with etched mineral surfaces. The preferred dissolution of feldspars might have caused the formation of Al-rich phases in the augite run, and the cloudy Si- and Al-rich phases within augite interstices represent alteration products of feldspar such as kaolinite. The orthopyroxene sample showed a slight enrichment of Fe and Mg.

The results of the experiments where augite reacted with distilled water showed the formation of fibrous reaction rims and strongly reacted inclusions (E1.1_H_A6, E1.2_H_A5, Fig. 5) that could have formed during leaching or the dissolution–precipitation process. The Al-rich bands of experiment E1.2_H_A5 could represent weathering products of feldspar. During the reaction of orthopyroxene with distilled water, the liquid moved along preexisting fractures that formed due to the mechanical stress during sample preparation. The liquid dissolved the pyroxene and thereby slightly increased the sizes of voids. Fe-rich acicular phases precipitated in the cavities (Fig. 5). It is important to

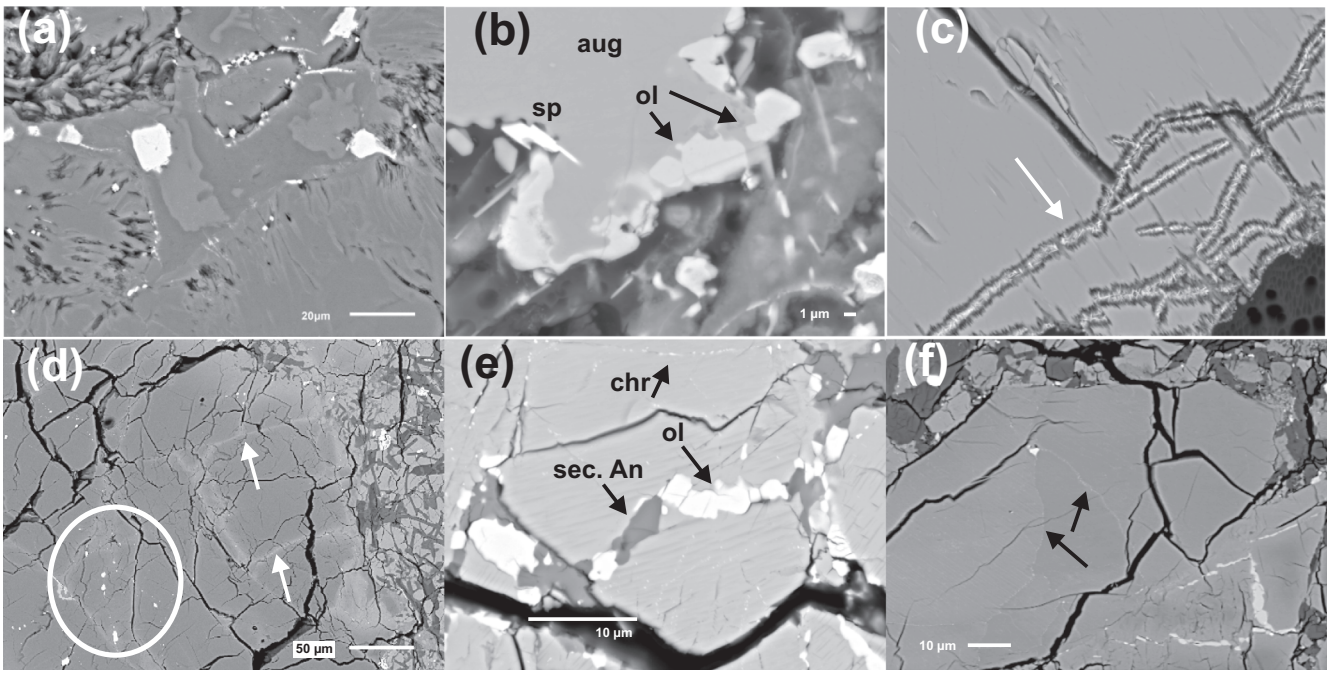

Fig. 7. BSE images of hydrothermal experiments (a–c) in comparison with natural pyroxenes in selected Yamato eucrites (Vollmer et al. 2020) that show textures of secondary alteration phases similar to experiments (d–f). a) Hydrothermal experiment of augite (aug) reacted with Fe-chloride solution (E1.1_H_A2, E1.2_H_A1), where Fe-rich phases, presumably magnetite, formed within the reaction product (arrow-marked). b) Hydrothermal experiment E1.2_H_A3, where Fe-rich olivine (ol) and spinel (sp) formed at the rim of pyroxene. c) Hydrothermal experiment E2_H_Hy, showing very fine spinel-like phases within pyroxene cracks (arrow-marked). d) Fe-enrichments along cracks within pyroxenes in eucrite Y-75011 (arrow-marked). However, single Fe-Ti-rich phases (encircled) also form, very similar to both heating (Fig. 6) and hydrothermal experiments (a). e) Well-developed fayalitic olivine, secondary anorthitic plagioclase (sec. An), and fine chromite phases (chr) crosscutting a pyroxene in eucrite Y-74159, similar to the experimental result in (b). f) Very fine chromite exsolution in pyroxene (Y-75011) (arrow-marked), roughly similar to experimental results in (c).

note here, that, in general, ferroan phases formed in almost every one of our hydrothermal experiments, even in those experiments with no additional supply of Fe by an Fe-rich liquid such as the runs with distilled water.

The results of the combined experiment (E4_H_Hy) also showed that ferroan phases formed without additional Fe added to the system. The Fe-enriched textures, which formed during the first heating step, disappeared, and we presume that these textures were destroyed by interaction with distilled water, leading to the formation of a wide reaction rim with Fe-Ti-rich, fibrous phases.

Formation of Secondary Ferroan Phases in HED Meteorites

The secondary Fe-enrichments and Fe-rich olivines in HED meteorites have been extensively studied and described (Takeda et al. 1983, 1994; Warren 2002; Barrat et al. 2011; Roszjar et al. 2011; Warren et al. 2014; Pang et al. 2017; Patzer and McSween 2018; Roszjar 2019; Vollmer et al. 2020) and the petrographic observations of previous studies can be summarized as follows. (1) Secondary Fe-enrichments and fayalitic olivines in HEDs are restricted to pyroxenes and absent in rock-forming plagioclase. (2) Fe-enrichments occur along preexisting cracks within pyroxene, and the cracks were caused either thermally or mechanically. (3) Fe-rich olivines partially fill fractures within pyroxenes and can also be observed at grain boundaries between pyroxene and plagioclase. They are usually accompanied by Fe-enrichments in the adjacent pyroxene. (4) The Fe-rich olivines usually have an irregular, granular shape. (5) Olivines do not exhibit typical features of replacement reactions, for example, irregular reaction rims or porosity. (6) Olivines are partially accompanied by Ca-rich plagioclase, troilite, chromite, SiO_2-polymorphs, merrillite, and apatite. (7) Pyroxenes containing these secondary features have variable textures and chemical compositions, e.g., magmatic zoning, equilibrated compositions, augite exsolution lamellae, or clouding. (8) Regions of mesostasis including Fe-rich olivine veins do not show signs of a re-melting process. (9) Rarely, olivine grains within veins exhibit 120° triple junctions indicative of thermal annealing. (10) Pyroxenes rarely show fine chromite segregation lamellae. (11) Fe-enrichments and Fe-rich olivine veins vary in extent and thickness from sample to sample and within grains therein. Previous studies discussed the formation of these features, including both high-temperature events and the influence of a liquid phase, and the next paragraph briefly summarizes these findings.

High-Temperature Processes

Takeda et al. (1983, 1994) described fayalitic olivine veins within unequilibrated pyroxenes in Y-75011 for the first time and considered a brief postmagmatic heating event, with a shock event as a possible scenario. They assumed that such a high-temperature event could have formed Fe-rich melts from mesostasis regions infiltrating pyroxene cracks. Another possible scenario involves the decomposition of Fe-rich pyroxene and subsequent formation of fayalite and SiO_2 phases. Warren (2002) examined Fe-rich olivine veins in the NWA 1000 basaltic eucrite and proposed a short-term heating event as the cause. Yamaguchi and Mikouchi (2005) and Yamaguchi et al. (2013) were the first to perform a series of melting experiments with basaltic eucrite material to document possible mineralogical and textural changes during such a heating event. They assumed that in case of a temperature rise slightly above the solidus of the eucrite material, small amounts of melts could form from phases with low melting temperatures. According to Stolper (1977), the solidus of eucrite material is at about 1100 °C, and Yamaguchi and Mikouchi (2005) and Yamaguchi et al. (2013) carried out experiments at temperatures of 1050 °C, 1070 °C, 1100 °C, and pressures of 1 atm. The duration was 24 h in each case and the oxygen fugacity was controlled to 1 log unit below the FeO-Fe oxygen buffer (fO_2 = IW−1) with a CO_2–H_2 gas mixture. Results at 1050 °C and 1070 °C showed that a small amount of melt (~1%) formed, enriched in Ti and P and located along grain boundaries, but also within mineral cracks. Mesostasis was fully preserved and, contrary to previous observations in eucrites, plagioclase was significantly more involved in the melting reactions than pyroxene. Experiments at 1100 °C showed >10 vol% melt in run products. At this temperature, ilmenite, Ca-phosphate, and areas of mesostasis were melted completely, while the initial, basaltic texture was still preserved. Newly formed fine-grained cristobalite needles, which presumably originated during quenching of the sample after completion of the experiment, were also observed. Plagioclase initially melted at its edges and showed widespread molten veins. Pyroxenes only remained as relicts and contained small pyroxene crystals, which probably formed during quenching. Other studies also argued that the melt product of mesostasis is highly mobile and strongly enriched in incompatible elements. However, such high levels of incompatible elements have not been found in Fe-enriched areas of natural samples (Barrat et al. 2007, 2011; Roszjar et al. 2011; Sarafian et al. 2013). In addition, Barrat et al. (2011) analyzed mesostasis in eucrites and neither found evidence for melting nor

areas of contact between mesostasis and olivine veins. The formation of secondary phases by melting of mesostasis can therefore be excluded, which limits the formation temperature of a heating event to a maximum of 1100 °C (Roszjar et al. 2011). Vollmer et al. (2020) also found no evidence for a contact between mesostasis and secondary phases in a study of polymict eucrites.

Our results of the heating experiments put important constraints on the formation temperature of the Fe-rich features in pyroxenes. For instance, results from experiment E1_S_Hy show textures similar to the Fe-rich veins in eucrites (Fig. 6). At a temperature of 1070 °C, which is only slightly above the peritectic point of orthopyroxene, fine Fe-Ti-rich veins formed along irregular fractures and symmetrically arranged cracks. The latter may follow crystal faces or microcracks along the cleavage of the crystal, the latter of which could have formed during preparation of the starting material cubes. However, Fe-accumulations within pyroxenes and olivines were not observed. At temperatures >1070 °C, the results of the experiments are texturally no longer similar to that observed in eucrites due to the high degree of melting. This implies that, in the case of a high-temperature event, formation conditions must be limited to a temperature only slightly above the peritectic temperature of the system.

Roszjar et al. (2011) discussed the formation of Fe-enrichments, olivine veinlets accompanied by anorthites and chromites in pyroxene by incongruent in situ melting of pyroxenes. Such an in situ melt requires a temperature slightly above the solidus of the primary Mg-rich pigeonite, which is about 1100 °C (Stolper 1977). Roszjar et al. (2011) assumed that such a heating process could have expired briefly in a magma chamber after the formation of the primary pyroxenes, but before ejection of the rock. During this short peritectic reaction, olivines could have formed and the remaining melt could have crystallized to Ca-rich plagioclase. This scenario would explain why observed features are restricted to pyroxenes and why feldspars are unaffected by such a short heating event (see experimental study by Yamaguchi and Mikouchi 2005; Yamaguchi et al. 2013). However, this hypothesis contradicts the observations and descriptions of Takeda et al. (1983, 1994) and Warren (2002), which show that secondary phases are significantly younger than the magmatic history of the rock. In addition, later studies, e.g., by Pang et al. (2017) and Vollmer et al. (2020), show that Fe-rich features occur in both unequilibrated and homogeneous pyroxenes, which is an exclusion criterion for the scenario of Roszjar et al. (2011). Furthermore, the Fe-rich features often accumulated in thermally or mechanically generated fractures of the pyroxenes and thus can only have formed after the first thermal overprint or mechanical brecciation event (Vollmer et al. 2020).

Newly formed Fe-Ti-rich phases in heating experiments of this study accumulated primarily along irregular fractures and formed symmetrical patterns (Figs. 2a and 2b). The Fe-enrichments observed in eucrites may also follow pyroxene cracks, but crystallographically controlled arrangements are absent. In order to make a statement about this difference between experiment and natural eucrite samples, first the cause for the symmetric arrangement in the experiments must be clarified. A second difference is the region inside the pyroxene next to the Fe-rich structures, which is usually accompanied by Fe-enrichment in natural samples. The results of heating experiments, however, show Fe-depletion in the adjacent pyroxene, independent of experimental duration and/or cooling rate. This argues against an in situ melt formation and more likely supports a process with an exogenous supplied and unknown medium being responsible for the deposition of Fe-rich material and that allows the diffusion of Fe into the pyroxene.

In some of the secondary olivine veins in HED meteorites (e.g., NWA 5073), small Cr-rich oxides were observed, which are according to Roszjar et al. (2011) of genetic importance. Vollmer et al. (2020) also observed Cr-rich phases as fine exsolution features in pyroxenes, whereas Pang et al. (2017) found them within olivine veins as granular minerals of a few μm sizes. The fine segregations, most likely chromites, are presumably the result of heating and partly texturally similar to the results of the high-temperature experiment E1_S_Hy (Fig. 2a). The granular chromites are always located next to or within olivine material indicating a common origin. Since Cr^{3+} has a high solubility in silicate melts but is immobile in aqueous liquids (Roeder and Reynolds 1991), it can be assumed that the formation process of the Cr-rich phases and therefore the formation of the accompanying olivine veins must be of magmatic origin (Roszjar et al. 2011). Pang et al. (2017) proposed an equilibrium temperature of 676–690 °C for an equilibrated association of Fe-rich olivine and chromite. These temperatures could be reached in a metamorphic event that occurred after the formation of the Fe-enrichments. Metamorphic events could also be responsible for the formation of Fe-rich diffusion veins, chromite exsolution lamellae, and maybe also for triple junctions of olivine grains in the veins (Pang et al. 2017). Furthermore, some of these enrichments might be caused by the interaction of late-stage residual Fe-rich magmatic fluids with previously crystallized (and, in some cases, metamorphosed)

eucritic igneous/volcanic rocks. One might argue that, because these features are also found in equilibrated pyroxenes, this requires the same postmagmatic metamorphic event. However, this could also occur when an equilibrated pyroxene from a metamorphosed lava flow was altered by interaction with late-stage fluids from an adjacent intrusive/extrusive body (e.g., Buchanan et al. 2000a,2000b).

The transitional regions from crystal to melt in experiments exposed to temperatures above 1070 °C showed that the elemental exchange distance increases with increasing duration at constant temperature. In other words, the longer the duration of a heating event, the greater the distance of the elemental reaction front. In terms of eucrites, the extent of Fe-enrichments could thus indicate the duration of a high-temperature event. However, since comparable Fe-enrichments did not occur in any of the heating experiments, the duration of such a process cannot be quantified here.

Since secondary alteration features are observed in both unequilibrated and equilibrated pyroxenes, formation of ferroan phases seems to be independent of the metamorphic degree. This raises the question of when these Fe-rich features formed, i.e., whether it was a single event or multiple events just before or after the last equilibration event. However, recent studies suggested that observed Fe-rich features likely formed in different areas of the host rock by a series of events and therefore during different evolutionary stages (e.g., Pang et al. 2017; Vollmer et al. 2020). The occurrence in primary, clearly unequilibrated pyroxenes observed in several basaltic eucrites further suggests that the formation of these features must be a postmagmatic, thermally independent process, since there is no other evidence of heating. Thus, these features may have formed by interaction with a liquid phase before, during, and after the equilibration of pyroxenes.

Hydrothermal Processes/Metasomatism

Some research suggests that the formation of secondary phases requires the influence of a postmagmatic metasomatic medium, presumably an Fe-rich liquid or a gas (steam/vapor; e.g., Mittlefehldt and Lindstrom 1997; Herd et al. 2004; Schwartz and McCallum 2005; Barrat et al. 2011; Pang et al. 2017). The interaction of such a liquid/gas with pyroxene could mobilize elements like Fe, Si, Mg, Mn, S, Ca, and Al and precipitate new phases elsewhere. The preserved magmatic zoning of pyroxenes indicates a short-term but efficient process in terms of cation transport. In the meteorite Serra de Magé, small quartz veins have been described that could have formed as precipitation products of an exogenous, SiO_2-mobilizing, aqueous solution (Treiman et al. 2004). Experimental work by Dohmen et al. (1998) shows that a dry vapor phase at high temperatures (>1300 °C) can coexist with solids and could also be an important transport medium for Fe, Mg, and Si. High-temperature steam could either degas globally during crust formation from the depth of the parent body or form by local volatilization of some elements during impact events (Schwartz and McCallum 2005). Vesta's magmatic gases could have a Moon-like composition, with CO_2, COS, CS, S_2, and a relatively high level of water (Fegley 1991; Fogel and Rutherford 1995; Sarafian et al. 2019). Fayalite could then be formed by the reaction between CO, metallic iron, and silica from the host rock (Equation 1; Brearley 1990).

$$2Fe^0_{(s)} + SiO_{2(s)} + 2CO_{(g)} = Fe_2SiO_{4(s)} + 2C_{(s)}) \quad (1)$$

Barrat et al. (2011) rejected this idea, because olivines in natural samples were not pure fayalites, but also contained a certain amount of Mg. Furthermore, only limited amounts of metallic Fe are found in a few eucrites, which they considered not sufficient to form the observed amounts of Fe-rich olivine as a reaction product. In addition, carbon and/or carbonate-containing phases would form in such a reaction, have not been reported in HED meteorites (Newton and Manning 2000; Treiman et al. 2004). Mittlefehldt and Lindstrom (1997) analyzed the chemistry of Fe-enrichments in pyroxenes, and their data show high Fe/Mn ratios, which more likely form during metasomatic instead of magmatic processes. Therefore, Mittlefehldt and Lindstrom (1997) concluded that Fe-enrichments were formed by a secondary interaction process with an Fe-rich liquid (FeO-metasomatism). In some carbonaceous and a few ordinary chondrites, aqueous liquids are considered as a metasomatic medium responsible for the formation of secondary fayalitic olivine (e.g., Krot et al. 1998, 2000; Jogo et al. 2009). Hua and Buseck (1995) described Fe-rich olivine as a direct condensate from a high-temperature oxidized nebular gas, while Krot et al. (1998, 2000) and Jogo et al. (2009) considered the Fe-rich deposition by a low-temperature aqueous solution to be more likely.

Aqueous liquids may have been episodically brought to the surface of a dry parent body by cometary impacts (Treiman et al. 2004; Greenwood et al 2011) or impacts by chondritic precursors (Warren et al. 2014). However, hydrous phases such as sheet silicates are likely to form during such reactions. In some areas of Vesta's surface, such phases were actually observed by the recent DAWN mission (Hasegawa et al. 2003; Prokof'eva-Mikhailovskaya et al. 2008), but they have not been detected within HED meteorites so far. Still,

fayalite may form from the reaction between H_2O and SiO_2 with metal and magnetite (Equation 2; Zolotov et al. 2006):

$$2Fe^0 + 2H_2O_{(g,l)} + SiO_{2(aq,s)} = Fe_2SiO_{4(s)} + 2H_2$$
$$Fe_3O_4 + SiO_{2(aq,s)} + 2H_{2(g,aq)} = Fe_2SiO_{4(s)} + Fe^0 + 2H_2O \quad (2)$$

According to Barrat et al. (2011), however, secondary fayalite cannot be produced at the expense of magnetite, since no magnetite has been found in eucrites so far. Furthermore, no evidence for the growth of fayalite and also of plagioclase at the expense of a primary phase could be observed. Secondary Ca-rich plagioclase formation thus may be the result of a dissolution–precipitation process, but textural evidence is missing here as well. One explanation for this lack of evidence could be direct destruction after the metasomatic process by thermal heating of the unequilibrated eucrites (Barrat et al. 2011).

Another possibility to form secondary phases is the import of elements from an exogenous source (Barrat et al. 2011) or by magma ocean degassing (Sarafian et al. 2017) followed by thermal metamorphism erasing those features in most samples. The type of liquid (aqueous or gaseous) as well as the chemical composition is still unknown and needs to be further investigated. The results of the hydrothermal experimental series in this work show that Fe-rich phases have formed in almost every experiment, irrespective of whether Fe was added to the liquid or not. Some textures of these experimental run products are comparable to that observed in eucrites (Fig. 7). This demonstrates that the metasomatic liquid alone could have served as a transport medium for elements and precipitate Fe-rich phases independently of its chemical composition. This could imply that the liquid composition is not the driving factor accounting for the formation of the secondary alteration features in eucrites.

The Fe-rich phases that formed during hydrothermal experiments have accumulated in previously thermally or mechanically generated fractures within pyroxenes. In most cases, those Fe-rich phases showed ilmenite- or spinel-like compositions. In the hydrothermal experiment E1.2_H_A3 (reaction of orthopyroxene with Fe-oxalate for 7 weeks), however, Fe-rich olivines have formed that texturally resemble secondary olivines in eucrites (Fig. 7b). They exhibit a granular morphology and are aligned along the pyroxene grain boundary. Their formation took place in areas where feldspar was adjacent to the pyroxene in the unreacted sample. The question therefore is whether feldspar was involved in the formation process of olivine, and whether its decomposition may have caused a change in the chemistry of the liquid responsible for the formation of secondary olivine. This is contradictory compared to that observed in eucrites, since secondary alteration features are restricted to pyroxenes, whereas feldspars appear completely unaffected. If the formation process of the secondary phases is a liquid reaction, feldspars should also show traces of that reaction. The formation of olivine at the expense of feldspar has not been previously observed in eucrites.

However, serpentine-like phases formed by the interaction of liquid and pyroxene in the experiment E1.2_H_A3 (Figs. 3d and 3e), which poses another problem. Serpentine has not been observed in eucrites yet. However, for some chondritic meteorites that likely underwent parent-body alteration, the absence of alteration products (e.g., phyllosilicates) is explained by prevailing temperatures of >200 °C (Brearley 2006; Brearley and Krot 2013), which could be the cause for eucrites as well that experienced widespread thermal metamorphism on the parent body (e.g., Metzler et al. 1995). In the case of aqueous alteration in eucrites, it is therefore possible that a thermal event could have overprinted any clear alteration products (Barrat et al. 2011).

Water in Eucrites

Eucrites are commonly characterized as magmatic rocks depleted of volatile elements (Papike 1998). However, visual and infrared spectra of Vesta's surface recorded by the DAWN mission (2011–2012) showed hydrated mineral phases (De Sanctis et al. 2012). Very recently, the influence of sulfur-induced metasomatism in deeper parts of the Vestan crust has been inferred from the analysis of the diogenite NWA 8321 (Zhang et al. 2020). Therefore, the influence of a volatile or aqueous medium originating from the interior of the parent body or the surface through OH-containing impactors cannot be ruled out (De Sanctis et al. 2012; Sarafian et al. 2014, 2017, 2019). Secondary ion mass spectrometry analyses have allowed in situ analyses of hydrogen isotopes in minerals such as apatite group minerals (Greenwood et al. 2011; Barnes et al. 2013; Sarafian et al. 2014, 2017). Ca-phosphates, including the apatite group minerals and merrillite, are the major volatile-containing minerals observed in eucrites so far (Sarafian et al. 2013, 2017; Roszjar et al. 2015). Sarafian et al. (2013, 2017), Roszjar et al. (2015), and Barrett et al. (2016) identified volatile concentrations including F, Cl, Br, I, and OH, of up to several wt% trapped in the crystal structures of accessory apatite and to a lesser extent in merrillite in HEDs. Many eucrites such as Nuevo Laredo, Stannern, or Serra de Magé contain almost pure fluorapatite, which presumably crystallized from a degassed magma, and apatite in the Moore County

meteorite occurs within pyroxenes (Sarafian et al. 2013). Presumably, they were in equilibrium with a relatively primitive (less-degassed) magma during formation, and clearly indicate the presence of H_2O on the parent body. The apatite grains of Juvinas fill out fractures and are associated with pyroxene and troilite. This observation clearly suggests formation by the influence of a high-temperature liquid. Furthermore, Sarafian et al. (2013) found that apatite composition shows no visible correlation with the degree of thermal metamorphism. It is generally believed that the HED parent body accreted mainly from anhydrous material (Boss 1998; Lucey et al. 2006), although some extant hydrous material was accreted to this and other volatile element-depleted bodies (e.g., Saal et al 2008; Sarafian et al 2017, 2019). There are other formation models that assume a mixture of various chondritic materials that included perhaps 30% CM-like and therefore water-rich material (Boesenberg and Delaney 1997). Furthermore, the vast majority of magmatic eucrites with crystallization ages of ~4.55 Ga already include volatile element-bearing apatites with OH in particular, which indicates that water must have been added relatively early. DAWN analyses show regions on Vesta's surface that are enriched in hydrated materials and regions that are depleted in them (De Sanctis et al. 2012). Higher OH absorption regions often have low albedo, and it is assumed that the dark material was brought to Vesta's surface by smaller impacts of primitive carbonaceous chondrites (Warren et al. 2014). However, bright areas also show low levels of OH and De Sanctis et al. (2012) assume that the OH-containing, uniformly distributed material was again obscured by later impacts. All of these observations imply that Vesta's crust contains heterogeneous distributions of volatile-rich materials that could therefore serve as agents for the possible metasomatic activities observed in HED meteorites.

We therefore conclude that the observed metasomatic reactions of pyroxenes from this experimental study, which could reproduce observed secondary alteration features, notably, ferroan-rich phases and Fe-enrichments in eucrite, indicate that the presence of early existing liquids on Vesta was likely and that temperature regimes below 1100 °C can lead to the formation of these secondary features. Our results further imply that this secondary alteration observed in the current HED suite of rocks that is limited to only a few dozen samples cannot be produced by short-time heating alone. Similar secondary Fe-rich veinlets have been reported recently within lunar samples (Warren et al. 2018; Zeng et al. 2020) implying that such metasomatic effects were common in nominally anhydrous bodies such as Vesta and the Moon. However, thermal metamorphism on Vesta might have erased those metasomatic features which may have formed in restricted areas on the parent body. Further experimental work involving a wider range of heating temperatures and hydrothermal experiments is required to test for a widespread formation process affecting a wider range of sample materials.

CONCLUSIONS

We performed a series of both heating and hydrothermal experiments on pyroxene material including augite and orthopyroxene minerals to further understand the formation of secondary ferroan phases in eucrites. The results of the heating experiments at slightly above the peritectic temperature of 1070 °C agree well with observed secondary features in natural eucrite, but higher temperature runs resulted in too much melt and therefore constrain the temperature of formation. Hydrothermal experiments also resulted in petrographic textures in good agreement with the Fe-rich features in eucrites. Hydrothermal experiments with fluids of different compositions, including Fe-rich aqueous liquids, distilled water, and HCl, indicate that the liquid only served as a metasomatic medium, since Fe-rich phases formed in almost every experiment, regardless of whether the liquid contained Fe or not. In one experiment, deposition of Fe-rich olivines, texturally similar to those observed in HED meteorites, occurred. We therefore conclude that the reaction of aqueous liquids with basaltic eucrite minerals is a plausible cause for the observed Fe-enrichments and formation of fayalitic olivine inside preexisting fractures of HED pyroxenes. However, the composition and origin of this liquid remain unknown. We further infer that Fe-rich alteration features cannot have formed by a single event, but rather by a combination of processes, e.g., influence of a liquid phase and high-temperature events. These complex alteration events must have taken place after the first crack-forming brecciation event of preexisting rock-forming silicates and before, during, and/or after equilibration of pyroxenes.

Acknowledgments—We thank G. Batic (NHM Vienna, Austria) and M. Trogisch (IfM, WWU Münster) for sample preparation. A.R.S. acknowledges support from a NASA Jenkins graduate fellowship (NNX13AR90H) and S.R. would like to thank the Heitfeld Foundation for support.

All authors have no conflict of interest to declare.

Data Availability Statement—Raw data will be stored on the respective instrument computers. All acquired

SEM data (TIFF images as well as spectrum images and/or tabbed spectrum files) will be stored on secure network servers within the University of Münster domain as well as on the non-commercial NRW cloud server "Sciebo" (https://www.sciebo.de).

Editorial Handling—Dr. Akira Yamaguchi

REFERENCES

Barnes J. J., Franchi I. A., Anand M., Tartèse R., Starkey N. A., Koike M., Sano Y., and Russell S. S. 2013. Accurate and precise measurements of the D/H ratio and hydroxyl content in lunar apatites using NanoSIMS. *Chemical Geology* 337–338:48–55.

Barrat J. A., Yamaguchi A., Greenwood R., Bohn M., Cotten J., Benoit M., and Franchi I. 2007. The Stannern trend eucrites: Contamination of main group eucritic magmas by crustal partial melts. *Geochimica et Cosmochimica Acta* 71:4108–4124.

Barrat J. A., Yamaguchi A., Bunch T. E., Bohn M., Bollinger C., and Ceuleneer G. 2011. Possible fluid-rock interactions on differentiated asteroids recorded in eucritic meteorites. *Geochimica et Cosmochimica Acta* 75:3839–3852.

Barrett T. J., Barnes J. J., Tartèse R., Anand M., Franchi I. A., Greenwood R. C., Charlier B. L. A., and Grady M. M. 2016. The abundance and isotopic composition of water in eucrites. *Meteoritics & Planetary Science* 51:1–15.

Binzel R. P. and Xu S. 1993. Chips off of asteroid 4 Vesta: Evidence for the parent body of basaltic achondrite meteorites. *Science* 260:186–191.

Binzel R. P., Gaffey M. J., Thomas P. C., Zellner B. H., Storrs A. D., and Wells E. N. 1997. Geologic mapping of Vesta from 1994 Hubble Space Telescope images. *Icarus* 128:95–103.

Boesenberg J. S. and Delaney J. S. 1997. A model composition of the basaltic achondrite planetoid. *Geochimica et Cosmochimica Acta* 61:3205–3225.

Boss A. P. 1998. Temperatures in protoplanetary disks. *Annual Review of Earth and Planetary Sciences* 26:53–80.

Bowen N. L. and Anderson O. 1914. The system MgO-SiO_2. *American Journal of Science (4th series)* 37:487–500.

Bowen N. L. and Schairer J. F. 1934. The system MgO-FeO-SiO_2. *American Journal of Science* 170:151–217.

Brearley A. J. 1990. Carbon-rich aggregates in type 3 ordinary chondrites: Characterization, origins, and thermal history. *Geochimica et Cosmochimica Acta* 54:831–850.

Brearley A. J. 2006. The action of water. In *Meteorites and the early solar system II*, edited by Lauretta D. S. and McSween H. Y. Jr. Tucson, Arizona: The University of Arizona Press. pp. 587–624.

Brearley A. J. and Krot A. N. 2013. Metasomatism in the early solar system: The record from chondritic meteorites. In *Metasomatism and the chemical transformation of rock*. Lecture notes in earth system sciences, edited by Harlov D. E. and Austrheim H. Berlin: Springer Verlag. pp. 659–789.

Buchanan P. C., Lindstrom D. J., Mittlefehldt D. W., Koeberl C., and Reimold W. U. 2000a. The South African polymict eucrite Macibini. *Meteoritics & Planetary Science* 35:1321–1331.

Buchanan P. C., Mittlefehldt D. W., Hutchison R., Koeberl C., Lindstrom D. J., and Pandit M. K. 2000b. Petrology of the Indian eucrite Piplia Kalan. *Meteoritics & Planetary Science* 35:609–615.

Cardew P. T. and Davey R. J. 1985. The kinetics of solvent-mediated phase transformations. *Proceedings of the Royal Society, London A* 398:415–428.

Consolmagno G. and Drake M. 1977. Composition and evolution of the eucrite parent body: Evidence from rare earth elements. *Geochimica et Cosmochimica Acta* 41:1271–1282.

De Sanctis M. C., Ammannito E., Capria M. T., Tosi F., Capaccioni F., Zambon F., Carraro F., Fonte S., Frigeri A., Jaumann R., Magni G., Marchi S., McCord T. B., McFadden L. A., McSween H. Y., Mittlefehldt D. W., Nathues A., Palomba E., Pieters C. M., Raymond C. A., Russell C. T., Toplis M. J., and Turrini D. 2012. Spectroscopic characterization of mineralogy and its diversity across Vesta. *Science* 336:697–700.

Denevi B. W., Blewett D. T., Buczkowski D. L., Capaccioni F., Capria M. T., De Sanctis M. C., Garry W. B., Gaskell R. W., Le Corre L., Li J. Y., Marchi S., McCoy T. J., Nathues A., O'Brien D. P., Petro N. E., Pieters C. M., Preusker F., Raymond C. A., Reddy V., Russell C. T., Schenk P., Scully J. E. C., Sunshine J. M., Tosi F., Williams D. A., and Wyrick D. 2012. Pitted terrain on Vesta and implications for the presence of volatiles. *Science* 338:246–249.

Dohmen R., Chakraborty S., Palme H., and Rammensee W. 1998. Solid-solid reactions mediated by a gas phase: An experimental study of reaction progress and the role of surfaces in the system olivine + iron metal. *American Mineralogist* 83:970–984.

Drake M. J. 1979. Geochemical evolution of the eucrite parent body: Possible nature and evolution of asteroid 4 Vesta? In *Asteroids*, edited by Gehrels T. Tucson, Arizona: The University of Arizona Press. pp. 765–782.

Drake M. J. 2001. The eucrite/Vesta story. *Meteoritics & Planetary Science* 36:501–513.

Fegley B. 1991. Thermodynamic models of the chemistry of lunar volcanic gases. *Geophysical Research Letters* 18:2073–2076.

Fogel R. A. and Rutherford M. J. 1995. Magmatic volatiles in primitive lunar glasses: I. FTIR and EPMA analyses of Apollo 15 green and yellow glasses and revision of the volatile-assisted fire-fountain theory. *Geochimica et Cosmochimica Acta* 59:201–215.

Gaffey M. J. 1997. Surface lithologic heterogeneity of asteroid 4 Vesta. *Icarus* 127:130–157.

Greenwood J. P., Itoh S., Sakamoto N., Warren P., Taylor L., and Yurimoto H. 2011. Hydrogen isotope ratios in lunar rocks indicate delivery of cometary water to the Moon. *Nature Geoscience* 4:79–82.

Grieg J. W. 1927. Immiscibility in silicate melts. *American Journal of Science (Series 5)* 13:1–44, 133–154.

Hasegawa S., Murakawa K., Ishiguro M., Nonaka H., Takato N., Davis C. J., Ueno M., and Hiroi T. 2003. Evidence of hydrated and/or hydroxylated minerals on the surface of asteroid (4) Vesta. *Geophysical Research Letters* 30:2123–2125.

Herd C. D. K., Treiman A. H., McKay G. A., and Shearer C. K. 2004. The behavior of Li and B during planetary basalt crystallization. *American Mineralogist* 89:832–840.

Hua X. and Buseck P. R. 1995. Fayalitic olivine in the Kaba and Mokoia carbonaceous chondrites. *Geochimica et Cosmochimica Acta* 59:563–578.

Jogo K., Nakamura T., Noguchi T., and Zolotov M. Y. 2009. Fayalite in the Vigarano CV3 carbonaceous chondrite: Occurrences, formation age and conditions. *Earth & Planetary Science Letters* 287:320–328.

Krot A. N., Petaev M. I., Scott E. R. D., Choi B. G., Zolensky M. E., and Keil K. 1998. Progressive alteration in CV3 chondrites: More evidence for asteroidal alteration. *Meteoritics & Planetary Science* 33:1065–1085.

Krot A. N., Brearley A. J., Petaev M. I., Kallemeyn G. W., Sears D. W. G., Benoit P. H., Hutcheon I. D., Zolensky M. E., and Keil K. 2000. Evidence for low-temperature growth of fayalite and hedenbergite in MacAlpine Hills 88107, an ungrouped carbonaceous chondrite related to the CM-CO clan. *Meteoritics & Planetary Science* 35:1365–1386.

Lucey P., Korotev R. L., Gillis J. J., Taylor L. A., Lawrence D., Campbell B. A., Elphic R., Feldman B., Hood L. L., and Hunten D. 2006. Understanding the lunar surface and space-moon interactions. *Reviews in Mineralogy and Geochemistry* 60:83–219.

McCoy T. J., Beck A. W., and Mittlefehldt D. W. 2014. Dawn's mission to asteroid 4-Vesta: Exploring a geologically and geochemically complex world. *Chemie der Erde—Geochemistry* 75:273–285.

Metzler K., Bobe K., Palme H., Spettel B., and Stöffler D. 1995. Thermal and impact metamorphism on the HED parent asteroid. *Planetary and Space Science* 43:499–525.

Mittlefehldt D. W. 2015. Asteroid (4) Vesta: I. The howardite-eucrite-diogenite (HED) clan of meteorites. *Chemie der Erde* 75:155–183.

Mittlefehldt D. W. and Lindstrom M. M. 1997. Magnesian basalt clasts from the EET 92014 and Kapoeta howardites and a discussion of alleged primary magnesian HED basalts. *Geochimica et Cosmochimica Acta* 61:453–462.

Newton R. C. and Manning C. E. 2000. Quartz solubility in H_2O-NaCl and H_2O-CO_2 solutions at deep crust-upper mantle pressures and temperatures: 2–15 kbar and 500–900°C. *Geochimica et Cosmochimica Acta* 64:2993–3003.

Pang R.-L., Zhang A.-C., and Wang R.-C. 2017. Complex origins of silicate veinlets in HED meteorites: A case study of Northwest Africa 1109. *Meteoritics & Planetary Science* 52:2113–2131.

Papike J. J. 1998. Comparative planetary mineralogy: Chemistry of melt-derived pyroxene, feldspar, and olivine. In *Planetary materials*, edited by Papike J. J. Reviews in Mineralogy, Vol. 36. Washington, D.C.: Mineralogical Society of America. pp. 7-1–7-11.

Patzer A. and McSween H. Y. 2018. Ferroan olivine-bearing eucrite clasts found in howardites. *Meteoritics & Planetary Science* 53:1131–1149.

Prettyman T. H., Mittlefehldt D. W., Yamashita N., Lawrence D. J., Beck A. W., Feldman W. C., McCoy T. J., McSween H. Y., Toplis M. J., Titus T. N., Tricarico P., Reedy R. C., Hendricks J. S., Forni O., Le Corre L., Li J. Y., Mizzon H., Reddy V., Raymond C. A., and Russell C. T. 2012. Elemental mapping by Dawn reveals exogenic H in Vesta's regolith. *Science* 338:242–246.

Prokof'eva-Mikhailovskaya V. V., Rublevskii A. N., and Bochkov V. V. 2008. Water combinations on the surface of the asteroid 4 Vesta. *Bulletin of the Crimean Astrophysical Observatory* 104:162–170.

Pun A. and Papike J. J. 1996. Unequilibrated eucrites and the equilibrated Juvinas eucrite: Pyroxene REE systematic and major, minor, and trace element zoning. *American Mineralogist* 81:1438–1451.

Putnis A. and Putnis C. V. 2007. The mechanism of re-equilibration of solids in the presence of a fluid phase. *Journal of Solid State Chemistry* 180:1783–1786.

Roeder P. L. and Reynolds I. 1991. Crystallization of chromite and chromium solubility in basaltic melts. *Journal of Petrology* 32:909–934.

Roszjar J. 2019. Secondary alteration of the Serra Pelada eucrite. *Meteoritics & Planetary Science* 54 (Suppl.):A6311.

Roszjar J., Metzler K., Bischoff A., Greenwood R. C., and Franchi I. A. 2009. Northwest Africa (NWA) 5073—An eucritic basalt with cm-sized pyroxenes (abstract). *Meteoritics & Planetary Science* 44 (Suppl.):A178.

Roszjar J., Metzler K., Bischoff A., Barrat J., Geisler T., Greenwood R. C., Franchi I. A., and Klemme S. 2011. Thermal history of Northwest Africa 5073—A coarse-grained Stannern-trend eucrite containing cm-sized pyroxenes and large zircon grains. *Meteoritics & Planetary Science* 46:1754–1773.

Roszjar J., John T., Kusebauch C., and Whitehouse M. J. 2015. Applying phosphate halogen compositions to trace magmatic or metamorphic fluids in inner solar system materials. *Geophysical Research Abstracts* 17:EGU 2015–14888.

Saal A. E., Hauri E. H., Cascio M. L., Van Orman J. A., Rutherford M. C., and Cooper R. F. 2008. Volatile content of lunar volcanic glasses and the presence of water in the Moon's interior. *Nature* 454:192–195.

Sarafian A. R., Roden M. F., and Patiño-Douce A. E. 2013. The volatile content of Vesta: Clues from apatite in eucrites. *Meteoritics & Planetary Science* 48:2135–2154.

Sarafian A. R., John T., Roszjar J., and Whitehouse M. J. 2017. Chlorine and hydrogen degassing in Vesta's magma ocean. *Earth and Planetary Science Letters* 459:311–319.

Sarafian A. R., Nielsen S. G., Marschall H. R., Gaetani G. A., Righter K., and Berger E. L. 2019. The water and fluorine content of 4 Vesta. *Geochimica et Cosmochimica Acta* 266:568–581.

Schwartz J. M. and McCallum I. S. 2005. Comparative study of equilibrated and unequilibrated eucrites: Subsolidus thermal histories of Haraiya and Pasamonte. *American Mineralogist* 90:1871–1886.

Stolper E. 1977. Experimental petrology of eucrite meteorites. *Geochimica et Cosmochimica Acta* 41:587–611.

Takeda H., Wooden J. L., Mori H., Delaney J. S., Prinz M., and Nyquist L. E. 1983. Comparison of Yamato and Victoria Land polymict eucrites: A view from mineralogical and isotopic studies. *Proceedings, 14th Lunar and Planetary Science Conference, Journal of Geophysical Research* 88:B245–B256.

Takeda H., Mori H., and Bogard D. D. 1994. Mineralogy and ^{39}Ar–^{40}Ar age of an old pristine basalt: Thermal history of the HED parent body. *Earth and Planetary Science Letters* 122:183–194.

Treiman A. H., Lanzirotti A., and Xirouchakis D. 2004. Ancient water on asteroid 4-Vesta: Evidence from a quartz veinlet in the Serra de Magé eucrite meteorite. *Earth and Planetary Science Letters* 219:189–199.

Vollmer C., Rombeck S., Roszjar J., Sarafian A. R., and Klemme S. 2020. The brecciated texture of polymict eucrites: Petrographic investigations of unequilibrated meteorites from the Antarctic Yamato collection. *Meteoritics & Planetary Science* 55:558–574.

Warren P. H. 2002. Northwest Africa 1000: A new eucrite with maskelynite, unequilibrated pyroxen crisscrossed by fayalite-rich veins, and Stannern-like geochemistry (abstract #1147). 33rd Lunar and Planetary Science Conference. CD-ROM.

Warren P. H., Rubin A. E., Isa J., Gessler N., Ahn I., and Choi B.-G. 2014. Northwest Africa 5738: Multistage fluid-driven secondary alteration in an extraordinarily evolved eucrite. *Geochimica et Cosmochimica Acta* 141:199–227.

Warren P. H., Isa J., Ebihara M., Yamaguchi A., and Baecker B. 2017. Secondary volatiles linked metallic iron in eucrites: The dual-origin metals of Camel Donga. *Meteoritics & Planetary Science* 52:737–761.

Warren P. H., Esposito R., and Manning C. 2018. Secondary, aqueous (?), metasomatic olivine veins in Apollo 14 mare basalt 1472 (abstract #2747). 49th Lunar and Planetary Science Conference. CD-ROM.

Yamaguchi A. and Mikouchi T. 2005. Heating experiments of the HaH 262 eucrite and implication for the metamorphic history of highly metamorphosed eucrites (abstract #1574). 36th Lunar and Planetary Science Conference. CD-ROM.

Yamaguchi A., Taylor G. J., and Keil K. 1996. Global crustal metamorphism of the eucrite parent body. *Icarus* 124:97–112.

Yamaguchi A., Mikouchi T., Ito M., Shirai N., Barrat J. A., Messenger S., and Ebihara M. 2013. Experimental evidence of fast transport of trace elements in planetary basaltic crusts by high temperature metamorphism. *Earth and Planetary Science Letters* 368:101–109.

Zeng X., Li S., Joy K. H., Li X., Liu J., Li Y., Li R., and Wang S. 2020. Occurrence and implications of secondary olivine veinlets in lunar highland breccia Northwest Africa 11273. *Meteoritics & Planetary Science* 55:36–55.

Zhang A.-C., Kawasaki N., Bao H., Liu J., Qin L., Kuroda M., Gao J.-F., Chen L.-H., Sakamoto N., and Yurimoto H. 2020. Evidence of metasomatism in the interior of Vesta. *Nature Communications* 11:1289–1296.

Zolotov M. Y., Mironenko M. V., and Shock E. L. 2006. Thermodynamic constraints on fayalite formation on parent bodies of chondrites. *Meteoritics & Planetary Science* 41:1775–1796.